inorganics

MDPI

Article

Capture Mechanism of Cadmium in Agricultural Soil Via Iron-Modified Graphene

Hongrui Wang [1,2], Junping Hu [3], Wentao Zhou [1], Pan Long [1], Xin Ma [4], Feng Zhang [5], Yuping Wu [6], Xiongwei Wu [5,*], Jiayu Dai [2,*] and Zhiqiang Fu [1,*]

1 College of Agronomy, Hunan Agricultural University, Changsha 410128, China
2 Department of Physics, National University of Defense Technology, Changsha 410128, China
3 College of Resource and Environmental, Hunan Agricultural University, Changsha 410128, China
4 Hunan Provincial Key Laboratory of Efficient and Clean Utilization of Manganese Resources, College of Chemistry and Chemical Engineering, Central South University, Changsha 410083, China
5 School of Chemistry and Materials Science, Hunan Agricultural University, Changsha 410128, China
6 School of Energy and Environment, Southeast University, Nanjing 211189, China
* Correspondence: wxw@hunau.edu.cn (X.W.); jydai@nudt.edu.cn (J.D.); zqf_cis@hunau.edu.cn (Z.F.)

Abstract: Cadmium (Cd) contamination in agricultural soils has caused extensive concern to researchers. Biochar with iron-compound modifications could give rise to the synergistic effect for Cd restriction. However, the related capture mechanism based on physicochemical properties is unclear. In this study, first principles calculations are proposed to explore the adsorption ability and potential mechanism of the ferric hydroxide modified graphene (Fe@G) for capturing $CdCl_2$. The simulation results show that the adsorption energy to $CdCl_2$ could enhance to −1.60 eV when $Fe(OH)_3$ is introduced on graphene. Subsequently, analyses of electronic properties demonstrated a significant electron transfer between Cd s-orbital and O p-orbital, thereby leading to strong adsorption energy. This theoretical study not only identifies a powerful adsorption material for Cd reduction in agricultural soils and reveals the capture mechanism of Fe@G for Cd but also provides a foundation and strategy for Cd reduction in agricultural soils.

Keywords: iron-modified biochar; cadmium; first principles calculation; capture mechanism; density functional theory

check for updates

Citation: Wang, H.; Hu, J.; Zhou, W.; Long, P.; Ma, X.; Zhang, F.; Wu, Y.; Wu, X.; Dai, J.; Fu, Z. Capture Mechanism of Cadmium in Agricultural Soil Via Iron-Modified Graphene. *Inorganics* **2022**, *10*, 150. https://doi.org/10.3390/inorganics10100150

Received: 25 August 2022
Accepted: 20 September 2022
Published: 22 September 2022

1. Introduction

With recent rapid developments and increased industrial emissions, cadmium (Cd) contamination is becoming a serious concern in east and south Asia, especially in China, India, and Thailand [1–4]. Here, until 2005, approximately 1.3×10^5 ha of agricultural soils in China were reported to be contaminated by Cd [5]. It is well known that Cd is a non-essential substance for plants; however, it is easily accumulated in agricultural crops [6–9]. For example, paddy rice can uptake Cd easily, and straw is the main accumulation region for Cd. A wide number of rice straws have been reportedly polluted by Cd every year in China [6,10]. In 2016, more than 10% of rice samples from rice markets exceeded the China National Standard for food contamination of Cd (<0.2 mg kg^{-1}) [11]. Furthermore, due to the 30 year biological half-life of Cd, it has the potential to cause serious medical conditions such as cancer and Itai-Itai disease [12–14]. Thus, it is necessary to reduce the availability of Cd in agricultural crops and consequently to the human system.

To date, in situ metal stabilization has raised considerable concern due to its high effect on reducing the bioavailability and toxicity of heavy metals in short periods [15–17]. Among them, biochar from pyrolysis with limited oxygen has an irregular aromatic structure, multi-layered accumulation forms, and unique physicochemical properties, which make it a great candidate for soil amendments to inhibit Cd in soils [18–21]. For instance, Luo et al. demonstrated that corncob biochar could significantly increase the total nitrogen

and organic matter content of the soil while stabilizing the availability of arsenic (As) and Cd in soil [22]. Furthermore, iron-based materials could reduce the efficiency of Cd by changing the physicochemical property of Cd [23,24]. Compared with pure biochar treatment, hybrid soil amendments of biochar and inorganic materials containing iron are better for reducing the Cd contamination of agricultural soils [18,25,26]. Qiao et al. reported that zero-valent iron (ZVI)-biochar could reduce Cd contamination in agricultural soils effectively [27]. Yin et al. reported that Fe-modified biochar reduced the accumulation of As and Cd in rice by reducing soil acidification [28]. However, the capture mechanism of Fe-modified biochar on Cd physicochemical systems has rarely been reported. Therefore, clarifying the capture mechanism of Fe-modified biochar on Cd is of paramount importance.

In this study, graphene (G) was used as the substrate to emulate the biochar. Graphene and its ferric hydroxide modification (Fe@G) were taken as the research objects to explore the capture mechanism with $CdCl_2$ by first principles calculations. First, the structural and electronic property differences between G and Fe@G were checked. Then, the adsorption ability of G and Fe@G with $CdCl_2$ were identified. Moreover, inherent changes in electronic properties and charge transferability were demonstrated. These findings show that there is a significant charge transfer between Fe@G and $CdCl_2$, which could be the main reason that Fe@G enhances the reduction of Cd. The calculation results will help to explain the capture mechanism of Fe-modified biochar and guide materials design for Cd reduction in agricultural soils.

2. Results and Discussion

Firstly, the structural stability and electronic properties of graphene were considered with modified ferric hydroxide ($Fe(OH)_3$) (Figures 1 and S1). The optimization structures of G and Fe@G were compared. There was a long distance from $Fe(OH)_3$ to G, which meant that a weak interaction existed between $Fe(OH)_3$ and G (Figure 1a,b). Furthermore, the electron localization function (ELF) diagram proved that although the electron property of G changed with the $Fe(OH)_3$ modification, there was no distinct electron exchange region between $Fe(OH)_3$ and G that would demonstrate that a physical adsorption effect exists (Figure 1c,d). Meanwhile, these results implied that G would not have a negative influence on $Fe(OH)_3$ to adsorb $CdCl_2$.

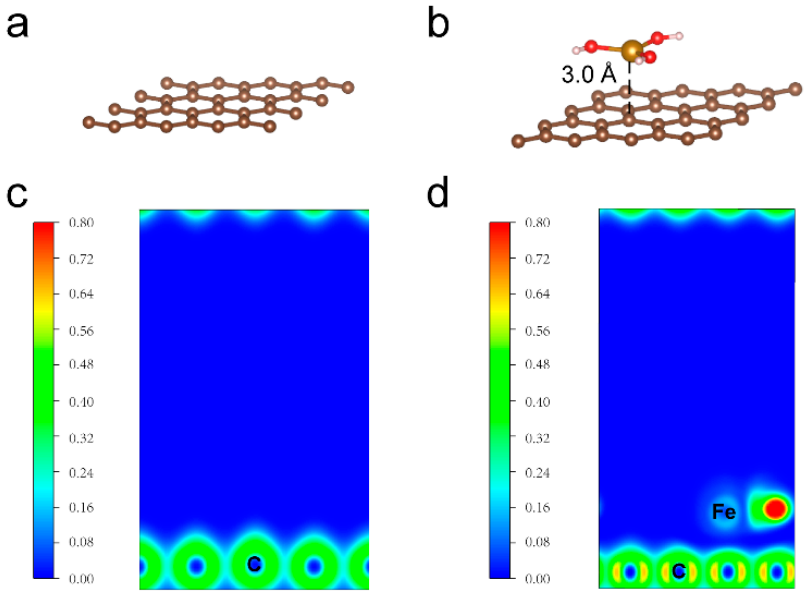

Figure 1. Schematic of G (**a**) and Fe@G (**b**), ELF diagram of G (**c**) and Fe@G (**d**).

To further explore the adsorption ability of $CdCl_2$ on G and Fe@G, the bond length (Cd-Cl), bond angle (Cl-Cd-Cl), and adsorption energy were considered. In previous studies, the long bond length and the large bond angle could facilitate the decomposition of the compound. Meanwhile, the weak adsorption energy could lead to the adsorption being unstable [29–31]. Compared with the pure $CdCl_2$ (179.56°) and that adsorbed on G (171.03°), the $CdCl_2$ showed the lowest bond angle (125.01°) when adsorbed on Fe@G (Figure 2a–c). Furthermore, in contrast to the pure $CdCl_2$ and adsorbed on G, the Fe@G possessed a longer bond length (2.95Å, Cd-Cl) near the $Fe(OH)_3$, whereas it had a shorter bond length (2.33Å, Cd-Cl) at the distance from $Fe(OH)_3$. This was substantial evidence that $CdCl_2$ would not decompose easily on Fe@G. Moreover, adsorption energies of G and Fe@G with $CdCl_2$ were taken for comparison. According to the computation formula of adsorption energy, the negative value implied a stronger restriction effect of $CdCl_2$ adsorbed on substrates [32]. Due to the weak physisorption of G and $CdCl_2$, G showed a poor adsorption ability (−0.42 eV), while Fe@G showed more negative values (−1.60 eV) when $CdCl_2$ was adsorbed (Figure 2d). The above results demonstrated that with the introduction of $Fe(OH)_3$, the Fe@G showed a considerable effect in restricting the migration of $CdCl_2$.

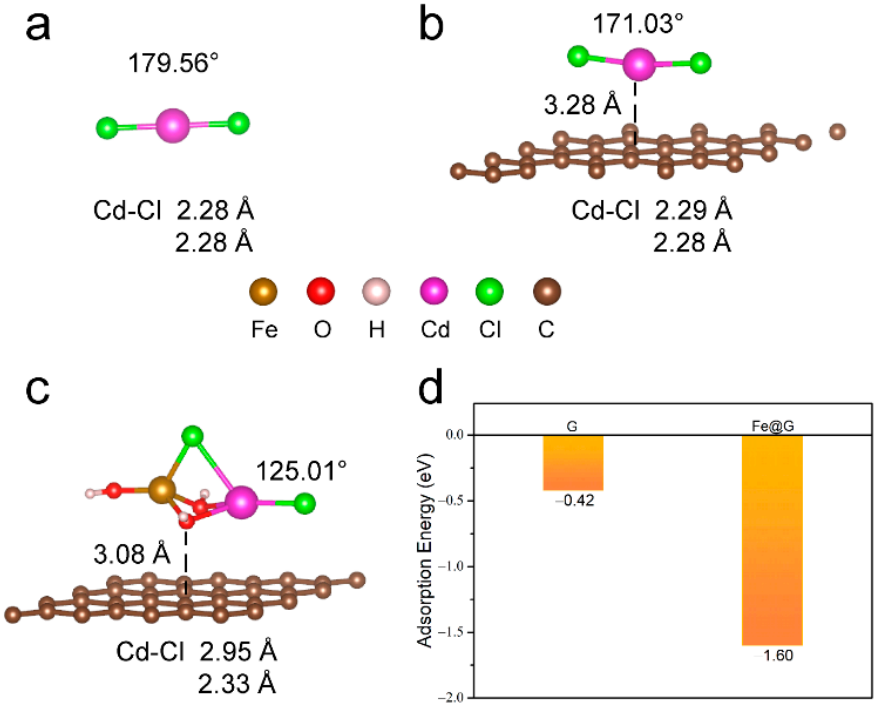

Figure 2. Schematic of pure $CdCl_2$ (**a**), $CdCl_2$ on G (**b**) and on Fe@G (**c**). (**d**) Adsorption energies of $CdCl_2$ on G and Fe@G.

Next, the electronic properties of $CdCl_2$ on G and Fe@G were investigated to gain an understanding of the inhibition mechanism of $CdCl_2$ on G and Fe@G. Initially, the electron charge density difference of $CdCl_2$ was drawn on G and Fe@G to probe the redistribution of charge. There was a clear charge depletion region between Cd and O atoms and a distinct charge accumulation region between Fe and Cl atoms, which indicated that a significant electron transfer occurred between the $CdCl_2$ and Fe@G (Figure 3b,d). However, this phenomenon was only expressed between the $CdCl_2$ and Fe@G interface. The adsorption configuration of $CdCl_2$ on G was no evidence of an obvious charge transfer between Cd or Cl and G, which may be the main reason for the weak adsorption ability of $CdCl_2$ on G (Figure 3a,c).

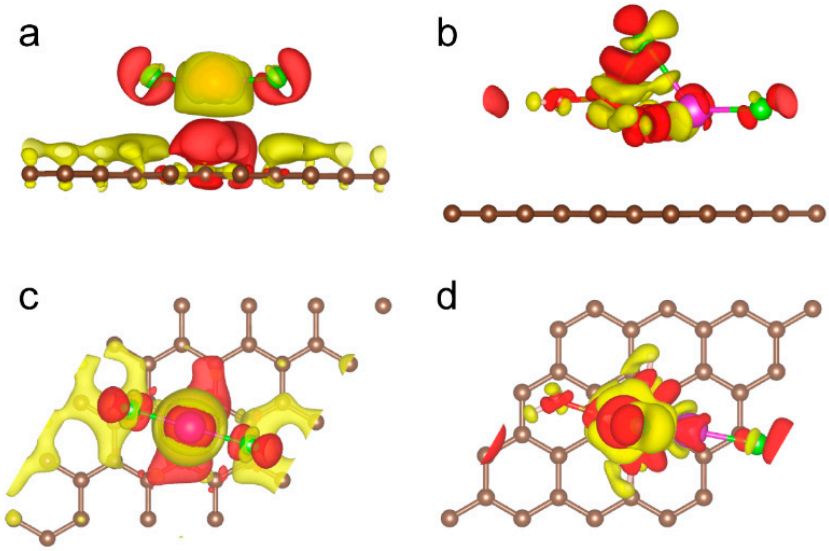

Figure 3. Charge density difference of the front views of $CdCl_2$ on G (**a**) and Fe@G (**b**), and the top views of $CdCl_2$ on G (**c**) and Fe@G (**d**). The isosurface is set to 3×10^{-4} e Å^{-3} in $CdCl_2$ on G and set to 3×10^{-3} e Å^{-3} in $CdCl_2$ on Fe@G. Note that yellow and red correspond to charge depletion and charge accumulation.

The above results are also observed in the ELF diagram (Figure 4). The $CdCl_2$ on G configuration had no distinct electron exchange between the $CdCl_2$ and G (Figure 4a). However, in contrast to G, the $CdCl_2$ on Fe@G configuration had a greater electron redistribution than the ELF diagram of pure Fe@G, where the localization degree of the electron for the -OH group near the Cd atom was reduced (Figure 4b,d). This phenomenon confirmed that $CdCl_2$ had influenced the electronic properties of $Fe(OH)_3$ in Fe@G, which also implied that a significant charge exchange existed between $Fe(OH)_3$ and $CdCl_2$. Next, the Bader charge analysis method was used to gain a deeper insight into the number of charges transferred between substrates and $CdCl_2$. Generally, more charges transferred expresses the higher restriction ability of the substrates to the molecules. Compared to the pure $CdCl_2$, the Cd site of the $CdCl_2$ on Fe@G configuration had an apparent charge transfer (0.141 e) that was higher than the $CdCl_2$ on G configuration (0.008 e) (Figure 4c). In addition, as shown in Table S1, the two Cl atoms in the $CdCl_2$ on Fe@G configuration also showed a charge exchange that was 0.05 e and 0.1 e greater than that of a Cl atom in pure $CdCl_2$. The reason for the significant difference in charge number between the two Cl atoms was ascribed to the different distances from $Fe(OH)_3$. Meanwhile, the total charge number of $CdCl_2$ in the $CdCl_2$ on Fe@G configuration showed a higher charge transfer than in other situations, and the results were consistent with Figures 3 and 4.

The above data show that the formation of the Cd-O and Fe-Cl bonds benefitted from charges transferred between $CdCl_2$ and the sorbent. However, in-depth studies must explore the reaction mechanism of $CdCl_2$ adsorption on Fe@G. Thus, the total density of states (DOS) and partial density of states (PDOS) of $CdCl_2$ on G and Fe@G configurations were investigated to gain a perspective on the interval states of energy and electron transfer (Figure 5). Differing from the $CdCl_2$ on G configuration (Figure 5a), there were prominent energy shifts that could be observed in the DOS of the $CdCl_2$ on Fe@G configuration, which means that the electron transfer had occurred under the adsorption situation as displayed in Figure 5b. Furthermore, the PDOS of the O and Cd atoms in the $CdCl_2$ on Fe@G configuration before and after adsorption were also considered. Due to the distinct charge donation of the Cd atom, the s-orbital of Cd exhibited a dramatic energy upshift after adsorption on Fe@G (Figure 5d). In contrast, the downshift of the p-orbital of O was evident, which was attributed to the O gain electrons when Fe@G interacted with $CdCl_2$. Meanwhile, these phenomena were also present in the Fe s-orbital and Cl p-orbital of the $CdCl_2$ on Fe@G configuration (Figure S2). However, there was no significant energy shift between

the C p-orbital and Cd s-orbital of the $CdCl_2$ on the G configuration (Figure 5c), which was consistent with the results of ELF, charge density difference, and Bader charge analysis.

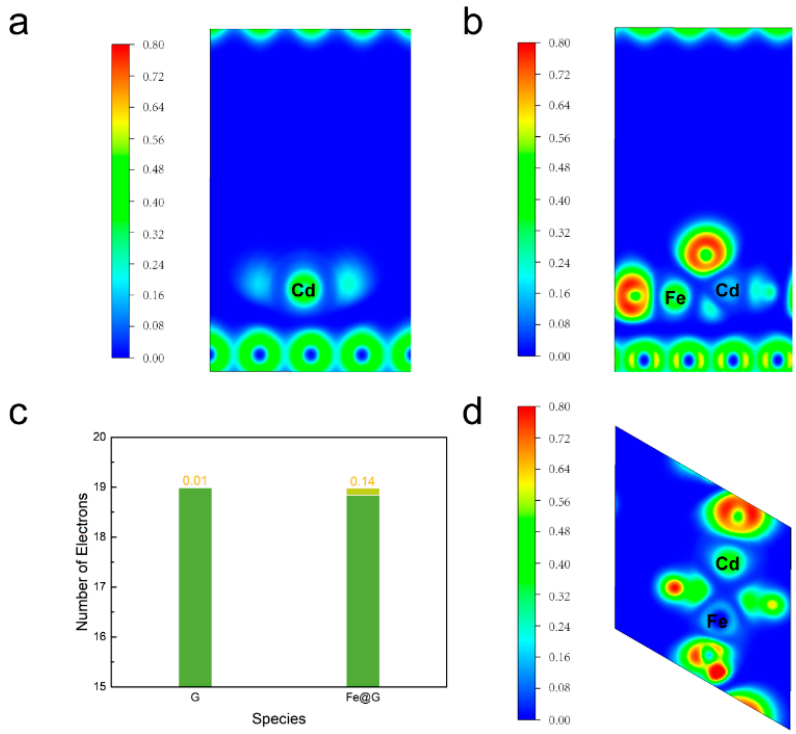

Figure 4. ELF diagram of $CdCl_2$ on G (**a**) and Fe@G (**b**). (**c**) The number of charge transfers of the Cd site for the $CdCl_2$ on substrates. Note that the dark and light green regions correspond to the number of electrons of the Cd for the $CdCl_2$ after adsorption on substrates, and the difference value with the electrons of the Cd for the pure $CdCl_2$, respectively. ELF diagram of top view of $CdCl_2$ on Fe@G (**d**).

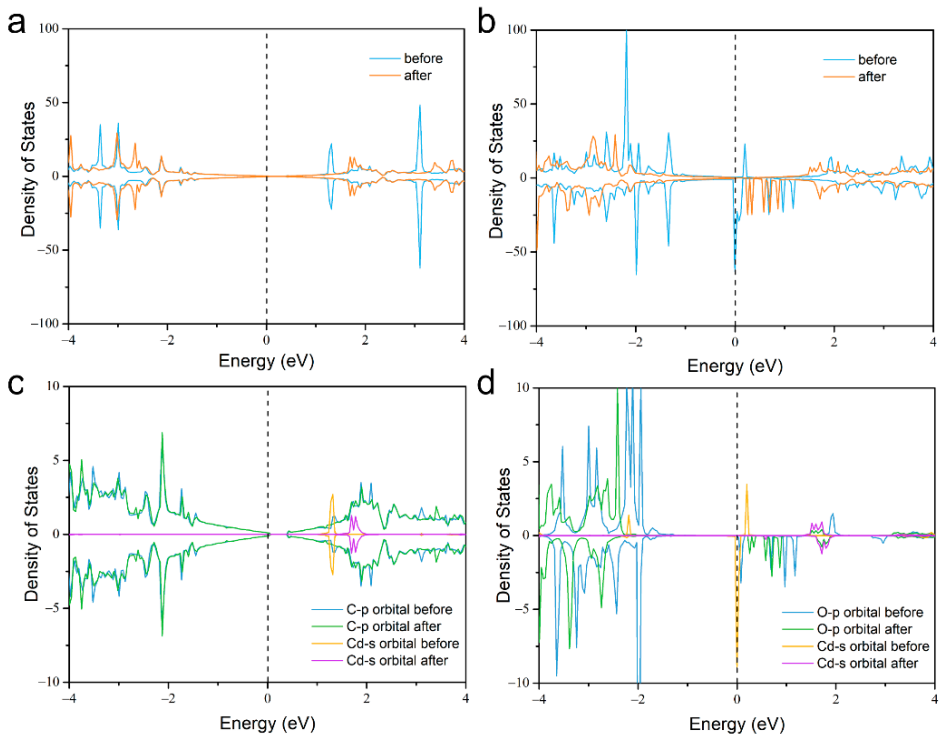

Figure 5. The density of states of $CdCl_2$ adsorbed on G (**a**) and Fe@G (**b**). The partial density of states of $CdCl_2$ adsorbed on G (**c**) and Fe@G (**d**).

3. Materials and Methods

The first principles calculations were carried out using the simulation software Vienna Ab initio Simulation Package (VASP) based on density functional theory (DFT) with the projector augmented wave (PAW) method [33–35]. Exchange-correction interactions were parameterized by the Perdew, Burke, and Ernzerhof (PBE) type, and DFT-D3 was used to consider the van der Waals interaction [36,37]. The energy cutoff was set to 500 eV, and convergence criteria for energy and force were set to 10^{-5} eV and 0.02 eV $Å^{-1}$ per atom, respectively. A vacuum layer with a thickness of 15 Å was employed to avoid interactions between the adjacent periodic units. The k-point was meshed by the Monkhorst–Pack method with a 3 × 3 × 1 grid for geometry optimizations and 11 × 11 × 1 grid for DOS calculation [38,39]. The calculations were computed within the DFT + U formalism to describe the localized d electrons, and the U values of Fe and Cd were set to 4 eV and 2 eV, respectively [40,41]. The adsorption energy (E_a) formula was defined as

$$E_a = E_{(Cd\text{-}substrate)} - (E_{Cd} + E_{substrate}), \quad (1)$$

where E_{Cd}, $E_{substrate}$, and $E_{(Cd\text{-}substrate)}$ represent the total energy of the $CdCl_2$, the substrates of G or Fe@G, and the energy of the $CdCl_2$ adsorption on the different substrates. The differential charge density ($\Delta\rho$) that was used to describe the charge distribution for the adsorption system is defined with the following formula [42]:

$$\Delta\rho = \rho_{Cd\text{-}substrate} - \rho_{substrate} - \rho_{Cd}, \quad (2)$$

where $\rho_{Cd\text{-}substrate}$, $\rho_{substrate}$, and ρ_{Cd} represent the charge density of the $CdCl_2$ adsorption on the different substrates, the substrates of G or Fe@G, and the $CdCl_2$. The electron localization function (ELF) diagram was drawn by VESTA [43].

4. Conclusions

In summary, we have revealed the capture ability and mechanism of $CdCl_2$ with $Fe(OH)_3$ modified graphene via first principles calculations. The $Fe(OH)_3$ modified carbon did not have a negative influence on adsorption of $CdCl_2$, and it could increase the chemisorption effect when the $Fe(OH)_3$ was introduced. This led to an adsorption energy improvement from −0.42 eV (G) to −1.60 eV. The adsorption behavior of Fe@G would then result in a large change in bond length (Cd-Cl) and bond angle (Cl-Cd-Cl) when $CdCl_2$ was adsorbed onto Fe@G. Furthermore, the electron charge density difference, ELF, and Bader charge analysis were used to confirm the charge transfer capacity. The Bader charge analysis displayed a 0.141 e charge transfer between Cd and Fe@G, which showed a greater amelioration over the $CdCl_2$ on G configuration. In addition, the electron transfer process was revealed by DOS and PDOS analysis. The PDOS proved that the Cd s-orbital and the O p-orbital exhibited a dramatic energy shift when the Fe@G interacted with $CdCl_2$, which provided powerful evidence for the capture mechanism of $CdCl_2$ with $Fe(OH)_3$ modified carbon. This study identified a powerful adsorption material for Cd reduction in agricultural soils and revealed the capture mechanism of Fe@G for Cd addition, showing potential as a strategy for Cd reduction in agricultural soils.

Supplementary Materials: The following supporting information can be downloaded at: https://www.mdpi.com/article/10.3390/inorganics10100150/s1, Figure S1: ELF diagram of the top view of Fe@G; Figure S2: The partial density of states of $CdCl_2$ adsorbed on Fe@G; Table S1: The number of charge transfers of the pure $CdCl_2$, and adsorbed on substrate.

Author Contributions: X.W., J.D. and Z.F.: conception and design of the study, approval of the version of the manuscript to be published; H.W. performed the study, analyzed the data, and wrote the manuscript; J.H., W.Z. and P.L. provided guidance on the data analysis; Y.W., F.Z. and X.M. revised the manuscript critically for important intellectual content. All authors have read and agreed to the published version of the manuscript.

Funding: This study is supported by the National Natural Science Foundation of China (Grant No. 31501277).

Institutional Review Board Statement: Not applicable.

Informed Consent Statement: Not applicable.

Data Availability Statement: Not applicable.

Acknowledgments: We thank the Agriculture and Rural Affairs Department of Hunan Province for their support of the research and demonstration of a high-efficiency rice model and disaster avoidance technology and the project of Breeding and Application of Rice Varieties with Low Cadmium Accumulation.

Conflicts of Interest: The authors declare no conflict of interest.

References

1. Kubier, A.; Wilkin, R.T.; Pichler, T. Cadmium in soils and groundwater: A review. *Appl. Geochem.* **2019**, *108*, 104388. [CrossRef] [PubMed]
2. Khan, M.; Khan, S.; Khan, A.; Alam, M. Soil contamination with cadmium, consequences and remediation using organic amendments. *Sci. Total Environ.* **2017**, *601*, 1591–1605. [CrossRef] [PubMed]
3. Mori, M.; Kotaki, K.; Gunji, F.; Kubo, N.; Kobayashi, S.; Ito, T.; Itabashi, H. Suppression of cadmium uptake in rice using fermented bark as a soil amendment. *Chemosphere* **2016**, *148*, 487–494. [CrossRef] [PubMed]
4. Wang, Q. Integrated amendment and ecological restoration of polluted soils by heavy metals. *Proc. Strategy Soil Environ. Prot. New Century China* **1998**, 26–29.
5. Du, Z.-Y.; Liu, Y.-J.; Tian, L.-X.; Wang, J.-T.; Wang, Y.; Liang, G.-Y. Effect of dietary lipid level on growth, feed utilization and body composition by juvenile grass carp (*Ctenopharyngodon idella*). *Aquac. Nutr.* **2005**, *11*, 139–146. [CrossRef]
6. Zong, Y.; Xiao, Q.; Lu, S. Biochar derived from cadmium-contaminated rice straw at various pyrolysis temperatures: Cadmium immobilization mechanisms and environmental implication. *Bioresour. Technol.* **2021**, *321*, 124459. [CrossRef]
7. Sun, L.; Wang, R.; Tang, W.; Chen, Y.; Zhou, J.; Ma, H.; Li, S.; Deng, H.; Han, L.; Chen, Y.; et al. Robust identification of low-Cd rice varieties by boosting the genotypic effect of grain Cd accumulation in combination with marker-assisted selection. *J. Hazard Mater.* **2022**, *424*, 127703. [CrossRef]
8. Satarug, S.; Moore, M. Adverse health effects of chronic exposure to low-level cadmium in foodstuffs and cigarette smoke. *Environ. Health Perspect* **2004**, *112*, 1099–1103. [CrossRef]
9. Haider, F.; Liqun, C.; Coulter, J.; Cheema, S.A.; Wu, J.; Zhang, R.; Ma, W.; Farooq, M. Cadmium toxicity in plants: Impacts and remediation strategies. *Ecotox Environ. Safe* **2021**, *211*, 111887. [CrossRef]
10. Shen, Z.; Fan, X.; Hou, D.; Jin, F.; O'Connor, D.; Tsang, D.C.W.; Ok, Y.S.; Alessi, D.S. Risk evaluation of biochars produced from Cd-contaminated rice straw and optimization of its production for Cd removal. *Chemosphere* **2019**, *233*, 149–156. [CrossRef]
11. Yang, W.-T.; Gu, J.-F.; Zou, J.-L.; Zhou, H.; Zeng, Q.-R.; Liao, B.-H. Impacts of rapeseed dregs on Cd availability in contaminated acid soil and Cd translocation and accumulation in rice plants. *Environ. Sci. Pollut Res.* **2016**, *23*, 20853–20861. [CrossRef] [PubMed]
12. Chaney, R. How does contamination of rice soils with Cd and Zn cause high incidence of human Cd disease in subsistence rice farmers. *Curr. Pollut. Rep.* **2015**, *1*, 13–22. [CrossRef]
13. Godt, J.; Scheidig, F.; Grosse-Siestrup, C.; Esche, V.; Brandenburg, P.; Reich, A.; Groneberg, D.A. The toxicity of cadmium and resulting hazards for human health. *J. Occup. Med. Toxicol.* **2006**, *1*, 22. [CrossRef] [PubMed]
14. Aoshima, K. Itai-itai disease: Renal tubular osteomalacia induced by environmental exposure to cadmium—historical review and perspectives. *Soil Sci. Plant Nutr.* **2016**, *62*, 319–326. [CrossRef]
15. Zanuzzi, A.; Faz, A.; Acosta, J. Chemical stabilization of metals in the environment: A feasible alternative for remediation of mine soils. *Environ. Earth Sci.* **2013**, *70*, 2623–2632. [CrossRef]
16. Rees, F.; Simonnot, M.; Morel, J. Short-term effects of biochar on soil heavy metal mobility are controlled by intra-particle diffusion and soil pH increase. *Eur. J. Soil Sci.* **2014**, *65*, 149–161. [CrossRef]
17. Xu, P.; Sun, C.-X.; Ye, X.-Z.; Xiao, X.-D.; Zhang, Q.; Wang, Q. The effect of biochar and crop straws on heavy metal bioavailability and plant accumulation in a Cd and Pb polluted soil. *Ecotox Environ. Safe* **2016**, *132*, 94–100. [CrossRef]
18. Rajendran, M.; Shi, L.; Wu, C.; Li, W.; An, W.; Liu, Z.; Xue, S. Effect of sulfur and sulfur-iron modified biochar on cadmium availability and transfer in the soil-rice system. *Chemosphere* **2019**, *222*, 314–322. [CrossRef]
19. Lehmann, J.; Rillig, M.; Thies, J.; Masiello, C.; Hockaday, W.C.; Crowley, D. Biochar effects on soil biota–a review. *Soil Biol. Biochem.* **2011**, *43*, 1812–1836. [CrossRef]
20. Zhang, X.; Wang, H.; He, L.; Lu, K.; Sarmah, A.; Li, J.; Baolan, N.S.; Pei, J.; Huang, H. Using biochar for remediation of soils contaminated with heavy metals and organic pollutants. *Environ. Sci. Pollut. Res.* **2013**, *20*, 8472–8483. [CrossRef]

21. Karami, N.; Clemente, R.; Moreno-Jiménez, E.; Lepp, N.; Beesley, L. Efficiency of green waste compost and biochar soil amendments for reducing lead and copper mobility and uptake to ryegrass. *J. Hazard. Mater.* **2011**, *191*, 41–48. [CrossRef] [PubMed]
22. Luo, M.; Lin, H.; He, Y.; Zhang, Y. The influence of corncob-based biochar on remediation of arsenic and cadmium in yellow soil and cinnamon soil. *Sci. Total Environ.* **2020**, *717*, 137014. [CrossRef] [PubMed]
23. Liu, R.; Altschul, E.; Hedin, R.; Nakles, D.; Dzombak, D.A. Sequestration enhancement of metals in soils by addition of iron oxides recovered from coal mine drainage sites. *Soil Sediment Contam.* **2014**, *23*, 374–388. [CrossRef]
24. Chen, S.; Chen, W.; Shih, C. Heavy metal removal from wastewater using zero-valent iron nanoparticles. *Water Sci. Technol.* **2008**, *58*, 1947–1954. [CrossRef]
25. Rehman, M.; Rizwan, M.; Khalid, H.; Ali, S.; Naeem, A.; Yousaf, B.; Liu, G.; Sabir, M.; Farooq, M. Farmyard manure alone and combined with immobilizing amendments reduced cadmium accumulation in wheat and rice grains grown in field irrigated with raw effluents. *Chemosphere* **2018**, *199*, 468–476. [CrossRef]
26. Guo, F.; Ding, C.; Zhou, Z.; Huang, G.; Wang, X. Effects of combined amendments on crop yield and cadmium uptake in two cadmium contaminated soils under rice-wheat rotation. *Ecotox Environ. Safe* **2018**, *148*, 303–310. [CrossRef]
27. Qiao, J.; Liu, T.; Wang, X.; Li, F.; Lv, Y.; Cui, J.; Zeng, X.; Yuan, Y.; Liu, C. Simultaneous alleviation of cadmium and arsenic accumulation in rice by applying zero-valent iron and biochar to contaminated paddy soils. *Chemosphere* **2018**, *195*, 260–271. [CrossRef]
28. Yin, D.; Wang, X.; Peng, B.; Tan, C.; Ma, L.Q. Effect of biochar and Fe-biochar on Cd and As mobility and transfer in soil-rice system. *Chemosphere* **2017**, *186*, 928–937. [CrossRef]
29. Zhou, G.; Zhao, S.; Wang, T.; Yang, S.Z.; Johannessen, B.; Chen, H.; Liu, C.; Ye, Y.; Wu, Y.; Peng, Y.; et al. Theoretical calculation guided design of single-atom catalysts towards fast kinetic and long-life Li-S batteries. *Nano Lett.* **2019**, *20*, 1252–1261. [CrossRef]
30. Gao, X.; Zhou, Y.; Liu, S.; Tan, Y.; Cheng, Z.; Shen, Z. FeN_3-embedded carbon as an efficient sorbent for mercury adsorption: A theoretical study. *Chem. Eng. J.* **2019**, *374*, 1337–1343. [CrossRef]
31. Hou, T.; Chen, X.; Peng, H.-J.; Huang, J.; Li, B.-Q.; Zhang, Q.; Li, B. Design Principles for Heteroatom-Doped Nanocarbon to Achieve Strong Anchoring of Polysulfides for Lithium-Sulfur Batteries. *Small* **2016**, *12*, 3283–3291. [CrossRef]
32. Dai, J.; Yuan, J. Modulating the electronic and magnetic structures of P-doped graphene by molecule doping. *J. Phys. Condens. Matter* **2010**, *22*, 225501. [CrossRef]
33. Hohenberg, P.; Kohn, W. Inhomogeneous Electron Gas. *Phys. Rev.* **1964**, *136*, B864. [CrossRef]
34. Kresse, G.; Furthmüller, J. Efficient Iterative Schemes for Ab Initio Total-Energy Calculations Using a Plane-Wave Basis Set. *Phys. Rev. B* **1996**, *54*, 11169. [CrossRef] [PubMed]
35. Kresse, G.; Furthmüller, J. Efficiency of ab-initio total energy calculations for metals and semiconductors using a plane-wave basis set. *Comput. Mater. Sci.* **1996**, *6*, 15–50. [CrossRef]
36. Perdew, J.; Burke, K.; Ernzerhof, M. Generalized Gradient Approximation Made Simple. *Phys. Rev. Lett.* **1996**, *77*, 3865. [CrossRef] [PubMed]
37. Zhang, F.; Guo, X.; Xiong, P.; Zhang, J.; Song, J.; Yan, K.; Gao, X.; Liu, H.; Wang, G. Interface Engineering of MXene Composite Separator for High-Performance Li-Se and Na-Se Batteries. *Adv. Energy Mater.* **2020**, *10*, 2000446. [CrossRef]
38. Froyen, S. Brillouin-zone integration by Fourier quadrature: Special points for superlattice and supercell calculations. *Phys. Rev. B* **1989**, *39*, 3168. [CrossRef]
39. Liu, Z.; Huang, T.; Chang, H.; Wang, F.; Wen, J.; Sun, H.; Hossain, M.; Xie, Q.; Zhao, Y.; Wu, Y. Computational Design of Single Mo Atom Anchored Defective Boron Phosphide Monolayer as a High-performance Electrocatalyst for the Nitrogen Reduction Reaction. *Energy Environ. Mater.* **2021**, *4*, 255–262. [CrossRef]
40. Zhou, J.; Sun, Q. Magnetism of phthalocyanine-based organometallic single porous sheet. *J. Am. Chem. Soc.* **2011**, *133*, 15113–15119. [CrossRef]
41. Ozugurlu, E. Cd-doped ZnO nanoparticles: An experimental and first-principles DFT studies. *J. Alloy Compd.* **2021**, *861*, 158620. [CrossRef]
42. Luo, J.; Sun, M.; Ritt, C.; Liu, X.; Pei, Y.; Crittenden, J.C.; Elimelech, M. Tuning Pb(II) Adsorption from Aqueous Solutions on Ultrathin Iron Oxychloride (FeOCl) Nanosheets. *Environ. Sci. Technol.* **2019**, *53*, 2075–2085. [CrossRef] [PubMed]
43. Momma, K.; Izumi, F. VESTA 3 for three-dimensional visualization of crystal, volumetric and morphology data. *J. Appl. Crystallogr.* **2011**, *44*, 1272–1276. [CrossRef]